Title

Preparatory meteorological modeling and theoretical analysis for a neighborhood-scale cool roof demonstration

Authors

Millstein, Dev

Levinson, Ronnen

Publication Date

2018-06-01

DOI

10.1016/j.uclim.2017.02.005

Peer reviewed

Preparatory Meteorological Modeling and Theoretical Analysis for a Cool Roof Field Test

Authors:

Dev Millstein, Ronnen Levinson

Energy Analysis and Environmental Impacts Division
Lawrence Berkeley National Laboratory

June 2018

The following manuscript is a preprint version of an article published in *Urban Climate*

DOI: http://dx.doi.org/10.1016/j.uclim.2017.02.005

This work was supported by the U.S.– China Clean Energy Research Center Building Energy Efficiency (CERC–BEE). The study was also supported by the Assistant Secretary for Energy Efficiency and Renewable Energy, Office of Building Technology, State, and Community Programs, of the U.S. Department of Energy (DOE), Lawrence Berkeley National Laboratory Contract No. DE-AC02-05CH11231. This research used resources of the National Energy Research Scientific Computing Center, a DOE Office of Science User Facility, supported by the Office of Science of the DOE under Lawrence Berkeley National Laboratory Contract No. DE-AC02-05CH11231.

DISCLAIMER

COPYRIGHT NOTICE

The following manuscript is a preprint version of the article:

Millstein, D. and Levinson, R., 2017. Preparatory meteorological modeling and theoretical analysis for a neighborhood-scale cool roof demonstration. *Urban Climate*. http://dx.doi.org/10.1016/j.uclim.2017.02.005

Preparatory Meteorological Modeling and Theoretical Analysis for a Cool Roof Field Test

Dev Millstein*, Ronnen Levinson

Heat Island Group, Lawrence Berkeley National Laboratory, Berkeley, California, 94720

Highlights

• We investigate the potential for a neighborhood-scale cool roof field test to provide measurable air temperatures changes.
• We develop a theoretical analysis of air temperature change based on an idealized heat transfer analysis.
• We compare the idealized heat transfer analysis to the outputs of a high resolution meteorological model.
• Both the idealized and the modeled analysis indicate a ~1 km2 neighborhood field test could provide an observable temperature signal.

Abstract

Replacing dark conventional roofs with more reflective “cool” roofs has been proposed as a method to lower urban air temperatures. Many meteorological studies have simulated potential cool roof air temperature reductions. However, economic and logistical challenges make it difficult to perform the large-scale demonstrations needed to verify these model results. This work assesses whether a neighborhood-scale cool roof demonstration could yield an observable air temperature change. We use both an idealized theoretical framework and a meteorological model to estimate the air temperature reduction that could be induced by increasing roof albedo over ~1 km2 area of a city. Both the idealized analysis and model indicate that an air temperature reduction could be detected, with the model indicating a reduction of 0.5 °C and the idealized analysis indicating a larger reduction of 1.3 °C. Follow-on modeling is recommended prior to design of a neighborhood-scale demonstration.

* Corresponding author

Keywords
Cool roofs
Urban heat island
Urban meteorology
Climate change adaptation

1 Introduction

”Cool” roofs reflect more of the sun's energy than do standard roofs. Increasing the albedo (solar reflectance) of a roof has been shown to save energy in a conditioned building, and to lower temperature in an unconditioned building (Gao et al., 2014). Urban climate models indicate that replacing a large portion of a city's standard roofs with cool roofs could reduce outside air temperature in that city (Rosenfeld et al., 1998; Millstein and Menon, 2011; Georgescu et al., 2014; Santamouris, 2014; Salamanca et al., 2016).

As part of the CERC-BEE Cool Roofs & Urban Heat Islands project, we have investigated the potential of cool roofs to decrease building energy use in China “directly” by reducing the envelope's solar heat gain (Gao et al., 2014). Cool roofs may also save energy “indirectly” by decreasing the air temperature difference across the building envelope. In many cities, meteorological models have been used to estimate the potential cooling of outdoor air from the replacement of all standard roofs (e.g., aged albedo 0.12) with cool roofs (e.g., aged albedo 0.65). For example, meteorological modeling showed that average summer daytime temperature reductions of about 1 °C could be achieved in Guangzhou, China (Cao et al., 2015). However, there have been no demonstrations performed, in Guangzhou or elsewhere, that could verify the modeled predictions of cool-roof induced city-wide air temperature changes, hereafter referred to as the “cool roof effect”. One partial exception to this statement is the analysis of cooling trends associated with the expansion of high-albedo greenhouse farming in a region in southeastern Spain (Campra et al., 2008). However, follow-on meteorological modeling indicated that only a portion of the historical temperature trends was likely associated with the expansion of high-albedo greenhouse farming; the remainder of the trend was unexplained (Campra and Millstein, 2013).

The reason that no field tests have been performed is the need to change a large portion of a city's roofing stock to produce a temperature signal large enough to observe—say, at least a few tenths of a degree Celsius. A small experiment encompassing a few buildings could quantify building cooling energy savings that result from reducing roof solar heat gain, but would not validate the meteorological models that show reductions to city-wide outside air temperatures.

On the other hand, expense and logistical challenges tend to make a city-wide test impractical. A demonstration would need to be larger than a few buildings but smaller than the scale of the city. This paper explores whether a neighborhood-scale (~1 km2) demonstration of cool roofs could produce a measurable reduction to air temperature. First, we perform an idealized heat transfer analysis that indicates that at typical urban wind speeds, air must flow over about 1 km of modified surface to yield a measurable change in near-ground air temperature. Next, we apply a meteorological model to simulate the impact on air temperature of altering roof albedo across 0.77 km2 sections of an urban area.

We employ a high-resolution regional weather and climate model (Weather Research and Forecasting, or WRF) to simulate ambient temperature changes from deployment of cool roofs to a small (0.8 km2) neighborhood of Guangzhou, China. The simulation uses a single-layer urban canopy model; it does not include specific building characteristics or a multilayer urban canopy model. This effort simply tests whether deploying cool roofs to an area ~1 km2 within the greater urban area of Guangzhou could

produce significant temperature changes within a simple modeling framework. While we have chosen to simulate the city of Guangzhou, the general results—meaning the change in daytime temperature per change in albedo—are likely applicable to many, but not all, urban areas. To support this statement, we point to the rough similarity in modeled temperature sensitivity across many U.S. cities (Millstein and Menon, 2011; Ban-Weiss et al., 2015) as well as Guangzhou China (Cao et al., 2015).

This test is necessary as modeling efforts to this date have generally been designed to evaluate large-scale, city-wide cool roof effects, but have not been designed to estimate changes from neighborhood-scale modifications. This exercise represents the first steps of developing a program to demonstrate the ability of reflective surfaces to cool cities. More complex modeling (such as work by Taleghani et al., 2016) should be pursued to increase the likelihood of the success of an actual demonstration. Specific suggestions for follow-on modeling are included in the concluding section of this paper.

2 Simplified heat transfer analysis

As air flows from a higher-albedo neighborhood to a lower-albedo neighborhood, the step change in surface albedo at the interface between neighborhoods will lead to a step change in surface temperature. Here we present a simple analytical model to estimate the air temperature change induced by a step change in the temperature of the surface over which it flows. We are particularly interested in the change in air temperature as a function of height above ground, and of distance from the point of the step change. This allows us to estimate the air flow distance needed to yield an observable change in air temperature at, say, 2 m above ground level. It thereby informs and complements our meteorological analysis.

This simplified analysis is provided only to estimate the characteristic length that air must travel over a surface for a step change in surface temperature to be detectable at a specified height above the surface. It models a long flat plate, and neglects variations in the elevation of the urban surface. It is an analog to air flow over open ground.

2.1 Heat transfer theory

Consider a free stream of air with uniform velocity u_∞ [m/s] and uniform temperature T_i [K] that strikes a long, thin, and infinitely wide plate at higher temperature T_0 [K]. We want to gauge the extent to which the air stream is warmed by the plate by evaluating the air temperature $T(x, y)$ [K] as a function of distance x [m] traveled along the plate and height y [m] above the plate (Fig. 1).

2.1.1 Differential equation

In the frame of the front of the air stream, the air can be approximated as a semi-infinite column with initial condition (IC)

$$T(y, t = 0) = T_i \tag{1}$$

and two boundary conditions (BCs): convective heat transfer at the plate

$$-k_e \left(\frac{\partial T}{\partial y}\right)_{y=0} = h[T_0 - T(y = 0, t)], \tag{2}$$

and constant temperature high above the plate:

$$T(y = \infty, t) = T_i. \tag{3}$$

Here $t = x/u_\infty$ [s] is the residence time of the air column over the plate, h [W/m²·K] is the convective heat transfer coefficient at the plate, and k_e [W/m·K], the air's effective thermal conductivity, is the sum of its molecular thermal conductivity k and its eddy thermal conductivity k_H. In the moving frame, the air temperature $T(y, t)$ is governed by the 1-D heat equation

$$\frac{\partial}{\partial y}\left[k_e \frac{\partial t}{\partial y}\right] = \rho c_p \frac{\partial T}{\partial t} \tag{4}$$

Where ρ [kg/m³] and c_p [J/kg·K] are the density and gravimetric specific heat of air.

This partial differential equation (PDE) can be expressed nondimensionally as

$$\frac{\partial}{\partial \hat{y}}\left[\hat{k}_e \frac{\partial \hat{t}}{\partial \hat{y}}\right] = \frac{\partial \hat{T}}{\partial \hat{t}} \tag{5}$$

where $\hat{y} \equiv y/y_0$, $\hat{t} \equiv t/t_0$, $\hat{T} \equiv (T - T_i)/(T_0 - T_i)$, and $\hat{k}_e \equiv k_e/k$ are the dimensionless height, time, temperature, and effective thermal conductivity; y_0 [m] is a characteristic height; $t_0 \equiv y_0^2/\alpha$ [s] is a characteristic time; and $\alpha \equiv k/\rho c_p$ [m²/s] is the molecular thermal diffusivity of air.

2.1.2 Characteristic height

To apply any solution of Eq. (5), we must establish a characteristic height, y_0. Following Kays and Crawford (1993), we define a characteristic height

$$y_0 = v/u_t \tag{6}$$

where v [m²/s] is the kinematic viscosity of air,

$$u_t = u_\infty \sqrt{c_f/2} \tag{7}$$

is friction velocity [m/s], and c_f is the dimensionless friction coefficient. Let dimensionless local Reynold's number

$$Re_x = x u_\infty / v. \tag{8}$$

Applying the Schultz-Grunow correlation for turbulent flow ($10^6 \le Re_x \le 10^9$),

$$c_f/2 = 0.185(log_{10} Re_x)^{-2.584}. \tag{9}$$

Therefore,

$$y_0 = \frac{v}{u_\infty \sqrt{0.185(log_{10} Re_x)^{-2.584}}}. \tag{10}$$

2.1.3 Effective thermal conductivity

Let ε_H [m²/s] and ε_M [m²/s] represent the eddy diffusivities for heat and momentum transfer, respectively. The air's eddy thermal conductivity

$$k_H \equiv \rho c_p \varepsilon_H = \rho c_p \left(\frac{\varepsilon_M}{Pr_t}\right) \tag{11}$$

where the dimensionless turbulent Prandtl number $Pr_t \equiv \varepsilon_M/\varepsilon_H$. In the fully turbulent region,

$$\frac{\varepsilon_M}{v} = \kappa \hat{y} \tag{12}$$

Where κ is the dimensionless von Kármán mixing-length constant (Kays and Crawford 1993). Substituting the dimensionless Prandtl number $Pr \equiv v/\alpha$ into Eqs. (11) and (12) yields

$$\frac{k_h}{k} = \left(\frac{Pr}{Pr_t}\right) \kappa \hat{y} \tag{13}$$

Therefore

$$\hat{k}_e = \frac{k_e}{k} = \frac{k + k_H}{k} = 1 + b\hat{y} \tag{14}$$

where constant

$$b \equiv \left(\frac{Pr}{Pr_t}\right) \kappa. \tag{15}$$

2.1.4 Convective heat transfer coefficient

The local forced convective heat transfer coefficient over a flat plate is

$$h_x = kNu_x/x \tag{16}$$

where k is the thermal conductivity of air and Nu_x is the local Nusselt number. Assume there is no unheated starting length. If the flow over the plate is laminar (Re_x < 500,000),

$$Nu_x = 0.332 Re_x^{1/2} Pr^{1/3} \tag{17}$$

If the flow over the plate is turbulent (Re_x > 500,000), then

$$Nu_x = 0.0296 Re_x^{4/5} Pr^{1/3} \tag{18}$$

(White 1988). Note that at a free-stream air speed of 2 m/s, an initially laminar flow will become turbulent (i.e., Re_x > 500,000) within 4 m.

2.1.5 Final system

The final dimensionless PDE is

$$\frac{d}{d\hat{y}}\left[(1+b\hat{y})\frac{\partial\hat{T}}{\partial\hat{y}}\right]=\frac{\partial\hat{T}}{\partial\hat{t}} \tag{19}$$

with dimensionless IC

$$\hat{T}(\hat{y},\hat{t}=0)=0 \tag{20}$$

and dimensionless BCs

$$-\left(\frac{\partial\hat{T}}{\partial\hat{y}}\right)=Bi_x[1-\hat{T}(\hat{y}=0,\hat{t})] \tag{21}$$

and

$$\hat{T}(\hat{y}=\infty)=0. \tag{22}$$

The local Biot number, $Bi_x = h_x y_0/k$, is evaluated with the transformation $x = u_\infty t$. Note that k, rather than k_e, appears in Bi_xbecause $k_e = k$ at the plate.

2.2 Heat transfer calculations

Using the transformations $\hat{y} = y/y_0$ and $\hat{t} = (\frac{x}{u_\infty})/t_0$, the dimensionless temperature profile $\hat{T}(x,y)$ was calculated at heights up to 100 m for air flowing at free-stream speeds of 1, 2, and 4 m/s over a plate of length 1,000 m.

Eqs. (19) through (22) were solved numerically with Mathematica 11.0.1.0 function NDSolve, using the method of lines (reduction of the PDE to a coupled set of ordinary differential equations in time). The characteristic height y_0 was evaluated halfway along the length of the plate (x = 500 m), and the constant temperature boundary condition specified in Eq. (22) was enforced at the top of the modeled domain (y =100 m). The maximum interval in dimensionless height $\hat{y}$ was set to limit to 0.01 m the maximum interval in dimensional height y. Following Kays and Crawford (1993), the mixing-length constant κ was set to 0.41, and the turbulent Prandtl number Pr_t was set to 0.85. The molecular properties of air were evaluated at 300 K and 1 atm.

2.3 Heat transfer results

At a wind speed of 2 m, the dimensionless air temperature $\hat{T}(x,y)$ 2 m above the plate is about 10^{-7} at 10 m, 0.025 at 100 m, and 0.207 at 1,000 m along the plate (**Figure 2**). Dimensionless air temperature versus dimensional height (up to 100 m) and dimensional distance (up to 1,000 m) is tabulated in in Appendix C (Supplementary data).

To apply this outcome, consider an air stream that has flowed for a very long distance over a "cool" ground surface with high albedo (ρ_i = 0.90) before striking a warmer plate of slightly lower albedo (ρ_0=0.60). Note the albedo change here (0.30) is similar to the average grid cell albedo change found in the meteorological modeling section (0.28), but of opposite sign; the magnitude of air temperature change is independent of the sign of the surface temperature change. We assume that on a typical summer day in Guangzhou, the peak solar irradiance is about 800 W/m^2. Assume that the small solar heat gain of the cool ground surface (about 80 W/m^2) is fully dissipated via thermal radiative exchange

with the sky. The ground surface will be at ambient near-ground air temperature (say, T_i = 310 K), and the air column striking the leading edge of the plate can be assigned uniform initial temperature $T(x=0, y) = T_i$.

Under low (0 to 2 m/s), medium (2 to 6 m/s), and high (6 to 10 m/s) wind conditions, ASTM Standard E1980-11: Standard Practice for Calculating Solar Reflectance Index of Horizontal and Low-Sloped Opaque Surfaces (ASTM, 2011) assigns to a horizontal surface a convective heat transfer coefficient of 5, 12, or 30 W/m^2·K, respectively. When solar irradiance is 800 W/m^2 and conduction through the surface is zero, the steady-state surface temperature balance expressed in Eq. (1) of ASTM E1980 predicts that a surface with solar reflectance 0.60 and thermal emittance 0.90 will be 20.3, 12.9, or 6.6 K warmer than an otherwise identical surface with solar reflectance 0.30 (Levinson, 2016). Of course, some heat will be conducted into the surface, diminishing temperature changes induced by solar heat gain. Hence, we assume that at the wind speed of 2 m/s used to compute the dimensionless air temperature shown in Fig. 2, the plate is about 10 K warmer than the long cool ground surface. The variation of building envelope surface temperature with albedo and/or wind speed is further discussed by Costanzo et al. (2014), Prado and Ferreira (2005), and Mirsadeghi et al. (2013).

If the plate is 10 K warmer than the ground surface ($T_0 - T_i$ = 10 K), the air temperature rise $T(x, y) - T_i$ at a height of 2 m will be about 10^{-7} × 10 K = 0.00 K at 10 m, 0.025 × 10 K = 0.25 K at 100 m, and 0.207 × 10 K = 2.1 K at 1000 m along the plate. For comparison to the modeling results presented in the next section, we look at a distance of 440 m along the plate. This is half the width of the altered neighborhood, representing the average temperature change rather than the temperature change at the downwind edge of the altered neighborhood. At 440 m along and 2 m above the plate, the air temperature rise will be about 0.131 × 10 K = 1.3 K. If the plate is 10 K cooler than the ground, 1.3 K will be the air temperature reduction at 440 m along and 2 m above the plate.

3 Modeling Methodology

To measure the effect of deploying cool roofs in a city, one would need to measure the outdoor air temperature at 2 m above ground level (AGL) in at least two neighborhoods of a city before and after cool roofs have been deployed in one of the neighborhoods. Without any albedo change we would expect the temperature difference between the neighborhoods to be consistent during the before and after periods, especially if the two periods occurred in the same year and season. However, if we alter the albedo of one neighborhood (neighborhood A) and not the other (neighborhood B), we would observe a cool roof effect on air temperature if the temperature difference $(A - B)_{period1}$ was significantly greater than the temperature difference $(A - B)_{period2}$, assuming period 2 occurs after the deployment of cool roofs. We followed this approach to simulate a neighborhood-scale cool roof demonstration. This is different from past meteorological modeling efforts designed to assess the effects of cool roof deployment on outdoor air temperature. The latter compare a modified run to a control run, both typically performed over the same time period.

3.1 Modeling setup

The meteorological simulations, including all sources of input data and physical parameterizations, were based on the modeling setup described by Cao et al. (2015). WRF version 3.6 was used. Note that recent releases to WRF have contained updates to the urban canopy model which could lead to some differences in the results if the analysis was rerun with the updated code. The new releases include updates related to hydrological processes within the urban canopy model, including specification of

urban irrigation and anthropogenic latent heat options (Yang et al., 2015), evaporation over impervious surfaces, and bug fixes. We have no reason to think the primary conclusions we derive from our modeling would change if rerun with the newer code. The modeling domain (shown in Fig. 3) contained five nests and was centered on the greater urban area of Guangzhou. The outermost domain was centered at 23.17° N and 113.33°E, with horizontal dimensions of 2,520 × 2,520 km and grid cell dimensions of 36 × 36 km. The four nested domains had grid cells with horizontal resolutions of 12, 4, 1.3, and 0.44 km respectively.

3.2 Modeling scenario design

In the fifth, most deeply nested domain (resolution of 0.44 km) we chose a neighborhood, hereafter called "COOL", in which to model the replacement of standard roofs with cool roofs (Fig. 3). It is important to note that in no way was this particular neighborhood ever considered for a specific field study; this location is just near the center of the greater Guangzhou urban area, and has relatively flat and homogeneous urban terrain. COOL is specified as a two-by-two block of grid cells with a combined width of 0.88 km and combined area of 0.77 km2. "CONTROL" represents unaltered areas of the city and is comprised of three non-contiguous grid cells that simulate the placement of three independent temperature monitors. All temperature comparisons described in the results section were made between the average temperatures across the four grid cells in COOL versus the average temperature across the three grid cells in CONTROL. We repeated this same experimental design four times, keeping the same time frame and domain definition but choosing different CONTROL and COOL areas. We chose four non-contiguous cells numbered 1 to 4. In the first trial, we specified COOL as a two-by-two block of cells in which the upper left corner of this block is cell 1. The remaining cells 2, 3, and 4 are CONTROL. In the next trial, the COOL block was moved so its upper left corner is at cell 2 and cells 1, 3, and 4 were CONTROL. This process was repeated a total of four times, so that the upper left corner of COOL could be located, in turn, at cell 1, 2, 3, or 4. Thus, each location highlighted in Fig. 3 was simulated separately as a COOL area and as a CONTROL area. We refer to each scenario by the relative location of the COOL area. For example, Fig. 3 shows the "upper-left corner" scenario.

We simulated 20 days in June 2005, and 20 days in July 2005. The June simulation represented the period prior to any cool roof deployment, and the July period represented the period post deployment, in which the four cells were altered to simulate the COOL neighborhood. The June and July simulations were not run continuously; instead, a series of five model runs was made for each month, June and July. Each run covered five days, overlapping the subsequent run by a day. This permitted the first day of each model run to be removed as spin-up time. In total 20 days per month, the 6th through the 25th of June and July, were available to be analyzed. We choose 5-day model runs to have simulations similar in length to the episodes modeled by Cao et al. (2015). Note that Cao et al. (2015) included a comparison of modeled and observed temperatures. We repeated the July model runs four times to simulate the location of the COOL neighborhood in each corner. The time-independent parameters (e.g., the land-use types and the orographic characterization) for the July run were kept exactly the same as the June run. The exception to this is the roof albedo in COOL, which was increased to 0.65 from 0.12. This raised the grid-cell average surface albedo in COOL to 0.39, up 0.28 from the CONTROL grid-cell average of 0.11.

3.3 Modeling results and discussion

Following Cao et al. (2015), we expect to see the largest signal of the cool roof effect during the day. This result is apparent in Figs. 4a, A1, A2, and A3. Specifically, we see that while June daytime peak temperatures in COOL often equal or exceed those in CONTROL, nearly all July daytime peak

temperatures in COOL are lower than those in CONTROL. This cool roof effect is also evident when comparing maps of average temperatures at 2 pm local standard time (LST) for June and July (Fig. 5).

The cool roof effect becomes even clearer when we examine the average diurnal cycle of temperature differences between COOL and CONTROL. Figs. 6 and B1 show that the strongest cool roof signal occurs during midday with peak temperature differences (COOL – CONTROL) reaching about -0.8 °C. We note the cooling seen in Fig. 4 looks remarkably similar to the shape and magnitude of cooling shown in Fig. 4a of Cao et al. (2015). This similarity occurs despite the fact that Cao et al. (2015) modeled cooling across the greater Guangzhou urban area and compared scenarios of the same time frame, but with different albedos.

Finally, we measure the statistical significance of these findings by comparing the average daytime (10:00 AM to 4:00 PM LST) temperature difference (COOL - CONTROL). We calculated 25 daytime temperature differences for each month, finding average and standard deviation values of 0.1 ± 0.35 °C in June and - 0.5 ± 0.39 °C in July for the upper-left corner scenario. As expected, because COOL and CONTROL share the same roof albedo in June but have different roof albedos in July, the air temperature difference between COOL and CONTROL is significant at the 95% level only for July. We found similar results for all three of the other COOL scenarios (Table 1).

Table 1. Mean and standard deviation of the difference in daytime (10:00 AM – 4:00 PM LST) temperature differences between COOL and CONTROL. Note that none of the June but all of the July means are statistically different from 0.0 at the 95% confidence level.

	June		July	
Scenario	mean (°C)	standard deviation (°C)	mean (°C)	standard deviation (°C)
Upper-left Corner	0.09	0.35	-0.54	0.39
Upper-right Corner	0.02	0.47	-0.70	0.28
Lower-right Corner	-0.08	0.30	-0.62	0.43
Lower-left Corner	-0.05	0.34	-0.60	0.25

The temperature reduction found in the idealized heat transfer analysis (1.3 °C) is larger than that modeled here (0.5 ± 0.39 °C), but of the same order of magnitude.

While the cool roof effect found here suggests that this experimental design would provide a useful field test of the ability of cool roofs to induce urban air temperature change, the overall modeling results also illustrate potential challenges to any future field experiment. For example, although it did not obscure results in this case, the spatial pattern of relative temperatures was not constant between time periods (Fig. 5), raising the possibility that other time periods or locations may not lead to such a clear cool roof effect. Another potential concern is that because only four grid cells were used in this modeling effort to represent COOL, intra-cell processes might swamp or degrade the signal found here.

Our analysis used WRF's "2-meter" output to obtain an average air temperature across each grid cell. The 2-meter temperature combines the temperatures above both streets and roofs while a thermometer would measure temperature either in an urban canyon or above a building roof. Thus, to recreate the experiment simulated here, air temperature would need to be measured in both the urban canyon and over rooftops. Our modeling effort does not identify possible differences between cooling within urban canyons and cooling above rooftops.

4 Conclusion

This analysis was designed as an initial screening exercise to evaluate whether a neighborhood-scale cool roof demonstration project (~1 km2) could produce measurable changes to outdoor air temperature. Both the idealized analysis and meteorological modeling support the hypothesis that a small field test could produce measurable results. The model predicts that one would find an average air temperature reduction of 0.5 ± 0.39 °C between 10:00 AM and 4:00 PM LST in the simulated scenario. Appropriate next steps would involve more complex follow-on modeling. This could include, in increasing order of complexity and expense, (1) the use of a multilayer urban canopy model incorporating specific building and road geometries; and (2) the use of large-eddy simulation to carefully represent temperature changes expected in a particular neighborhood. The follow-on effort would provide additional insight into the temperature effects of neighborhood albedo modification prior to final design of a demonstration.

Acknowledgements

The authors would like to express their thanks for support from the U.S.–China Clean Energy Research Center Building Energy Efficiency Consortium (CERC–BEE). The study was also supported by the Assistant Secretary for Energy Efficiency and Renewable Energy, Office of Building Technology, State, and Community Programs, of the U.S. Department of Energy (DOE), under Contract DE-AC02-05CH11231. This research used resources of the National Energy Research Scientific Computing Center, a DOE Office of Science User Facility, supported by the Office of Science of the DOE under Contract DE-AC02-05CH11231.

References

ASTM, 2011. ASTM E1980-11: Standard Practice for Calculating Solar Reflectance Index of Horizontal and Low-Sloped Opaque Surfaces. ASTM International, West Conshohocken, PA http://dx.doi.org/10.1520/E1980-11.

Ban-Weiss, G.A., Woods, J., Millstein, D.E., Levinson, R., 2015. Using remote sensing to quantify albedo of roofs in seven California cities, Part 2: Results and application to climate modeling. Sol. Energy 115:791–805. http://dx.doi.org/10.1016/j.solener.2014.10.041.

Campra, P., Millstein, D., 2013. Mesoscale climatic simulation of surface air temperature cooling by highly reflective greenhouses in SE Spain. Environ. Sci. Technol. 47 (21):12284–12290. http://dx.doi.org/10.1021/es402093q.

Campra, P., Garcia, M., Canton, Y., Palacios-Orueta, A., 2008. Surface temperature cooling trends and negative radiative forcing due to land use change toward greenhouse farming in southeastern Spain. J. Geophys. Res. 113, D18109. http://dx.doi.org/10.1029/2008JD009912.

Cao, M., Rosado, P., Lin, Z., Levinson, R., Millstein, D., 2015. Cool roofs in Guangzhou, China: Outdoor air temperature reductions during heat waves and typical summer conditions. Environ. Sci. Technol. 49 (24):14672–14679. http://dx.doi.org/10.1021/acs.est.5b04886.

Gao, Y., Xu, J., Yang, S., Tang, X., Zhou, Q., Ge, J., Xu, T., Levinson, R., 2014. Cool roofs in China: Policy review, building simulations, and proof-of-concept experiments. Energy Policy 74:190–214. http://dx.doi.org/10.1021/acs.est.5b04886.

Georgescu, M., Morefield, P.E., Bierwagen, B.G., Weaver, C.P., 2014. Urban adaptation can roll back warming of emerging megapolitan regions. Proc. Natl. Acad. Sci. U. S. A. 111 (8):2909–2914. http://dx.doi.org/10.1073/pnas.1322280111.

Kays, M., Crawford, M.E., 1993. Convective Heat and Mass Transfer. McGraw-Hill.

Levinson, R., 2016. SRI Calculator. Heat Island Group, Technical Resources. Lawrence Berkeley National Laboratory, Berkeley, CA http://heatisland.lbl.gov/resources/technical-resources.

Millstein, D., Menon, S., 2011. Regional climate consequences of large-scale cool roof and photovoltaic array deployment. Environ. Res. Lett. 6:034001. http://dx.doi.org/10.1088/17489326/6/3/034001.

Rosenfeld, A.H., Akbari, H., Romm, J.J., Pomerantz, M., 1998. Cool communities: strategies for heat island mitigation and smog reduction. Energ. Buildings 28:51–62. http://dx.doi.org/10.1016/S03787788(97)00063-7.

Salamanca, F., Georgescu, M., Mahalov, A., Moustaoui, M., Martilli, A., 2016. Citywide impacts of cool roof and rooftop solar photovoltaic deployment on near-surface air temperature and cooling energy demand. Bound. Layer Meteorol. 161 (1):203–221. http://dx.doi.org/10.1007/s10546-016-0160y.

Santamouris, M., 2014. Cooling the cities - A review of reflective and green roof mitigation technologies to fight heat island and improve comfort in urban environments. Sol. Energy 103:682–703. http://dx.doi.org/10.1016/j.solener.2012.07.003.

Taleghani, M., Sailor, D., Ban-Weiss, G.A., 2016. Micrometeorological simulations to predict the impacts of heat mitigation strategies on pedestrian thermal comfort in a Los Angeles neighborhood. Environ. Res. Lett. 11:024003. http://dx.doi.org/10.1088/1748-9326/11/2/024003.

White, F.M., 1988. Heat and Mass Transfer. Addison-Wesley.

Yang, J., Wang, Z-Hu, Chen, F., Miao, S., Tewari, M., Voogt, J.A., Myint, S., 2015. Enhancing hydrologic modelling in the coupled weather research and forecasting-urban modelling system. Bound.-Layer Meteorol. 155:87–109. http://dx.doi.org/10.1007/s10546-014- 9991-6.

Figures:

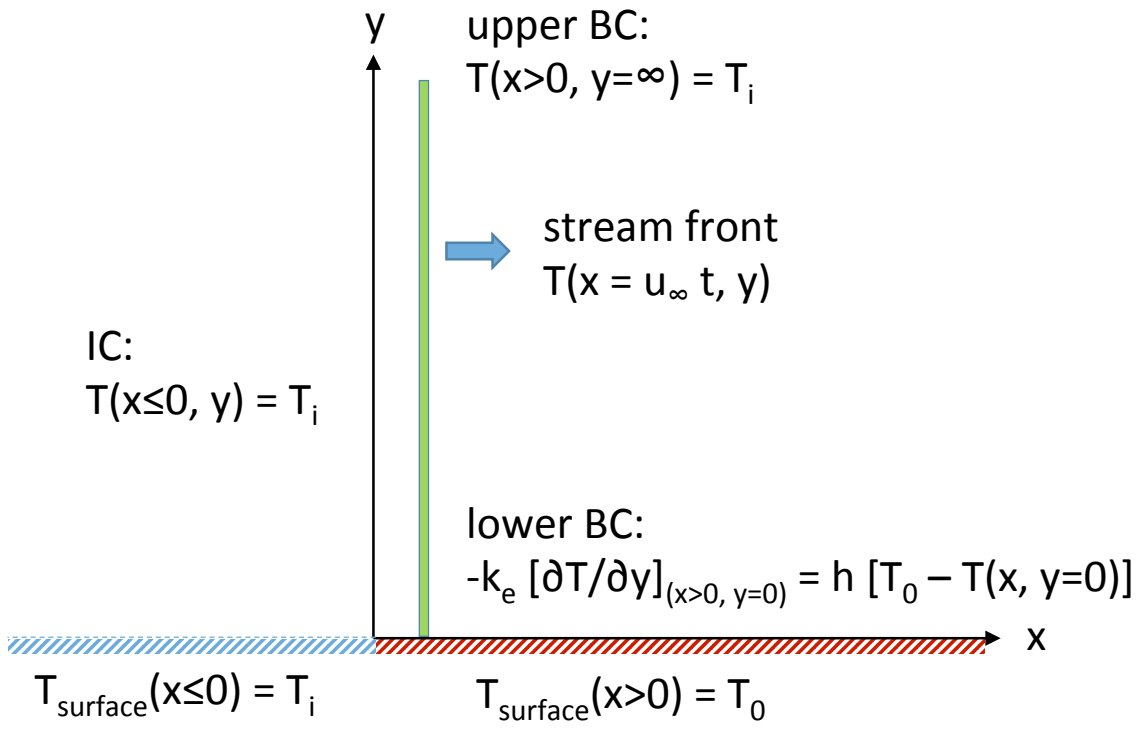

Figure 1. Sketch of air stream traveling over flat plate, passing surface temperature discontinuity at x = 0.

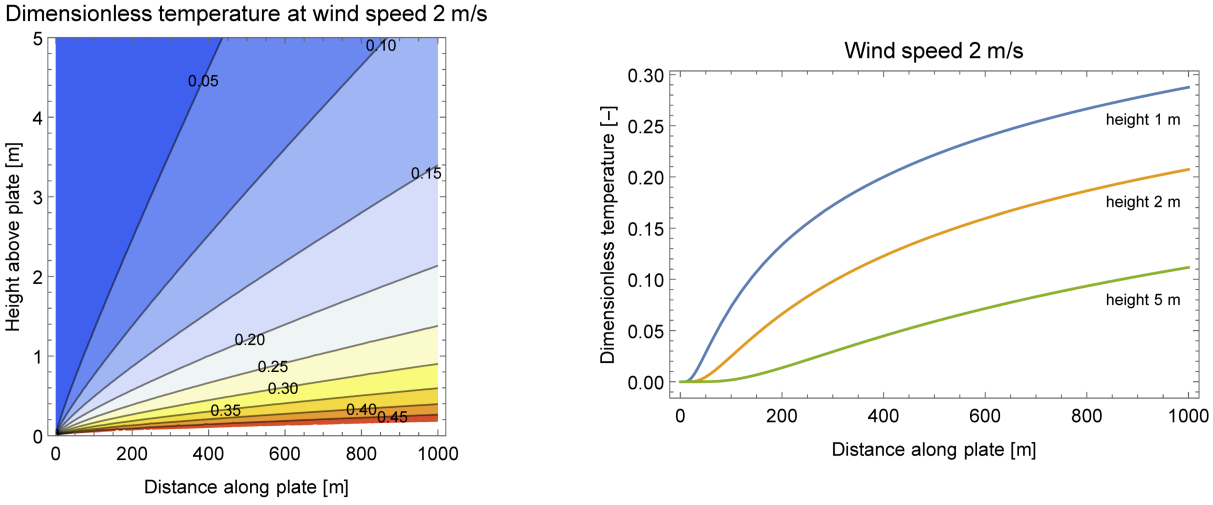

Figure 2. Variation with dimensional distance along plate (x) and dimensional height above plate (y) of the dimensionless temperature $\hat{T}(x, y)$ of air flowing at 2 m/s over a 1 km long flat plate. At left, general contours; at right, values at heights of 1, 2, and 5 m.

A

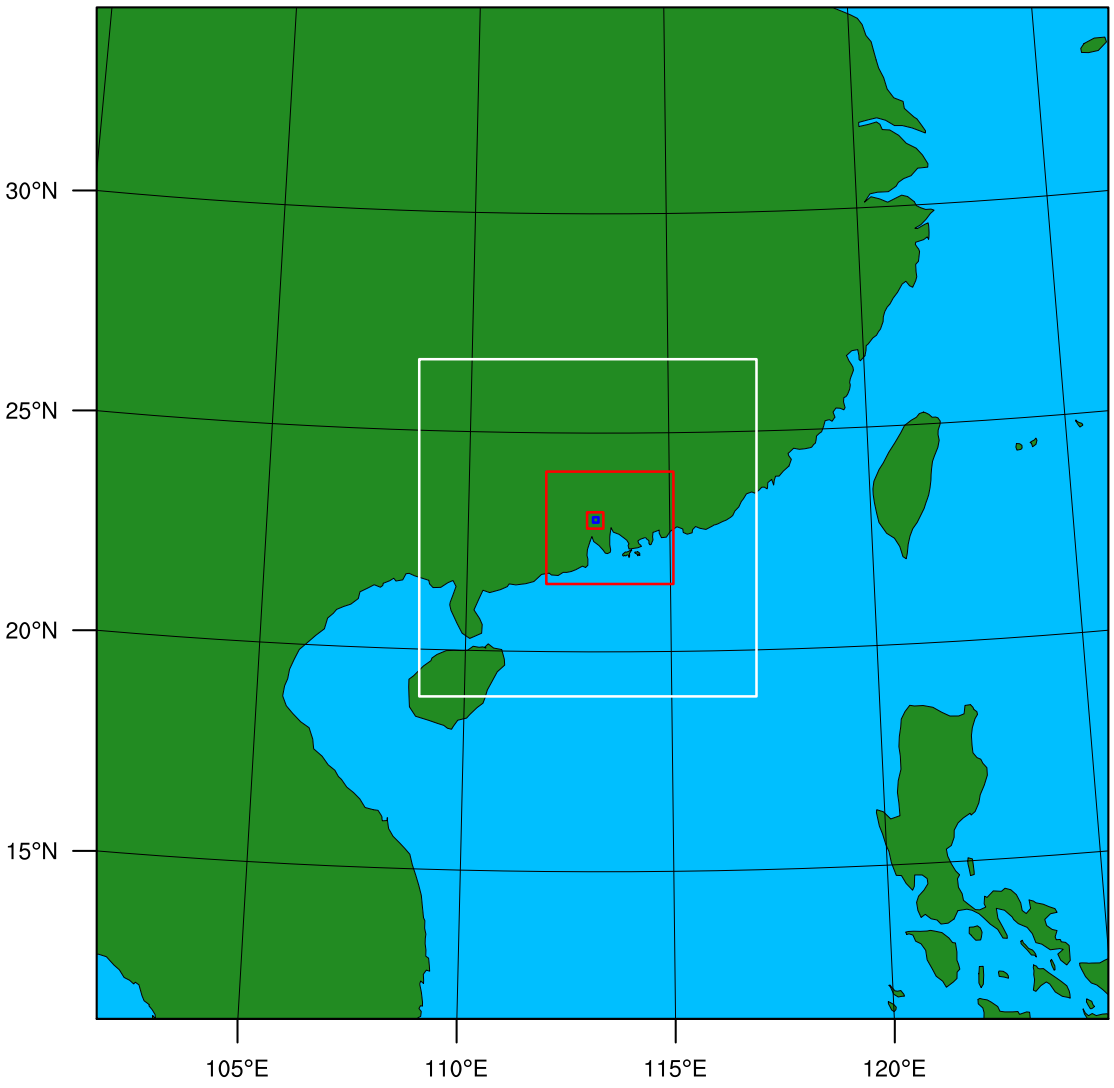

B

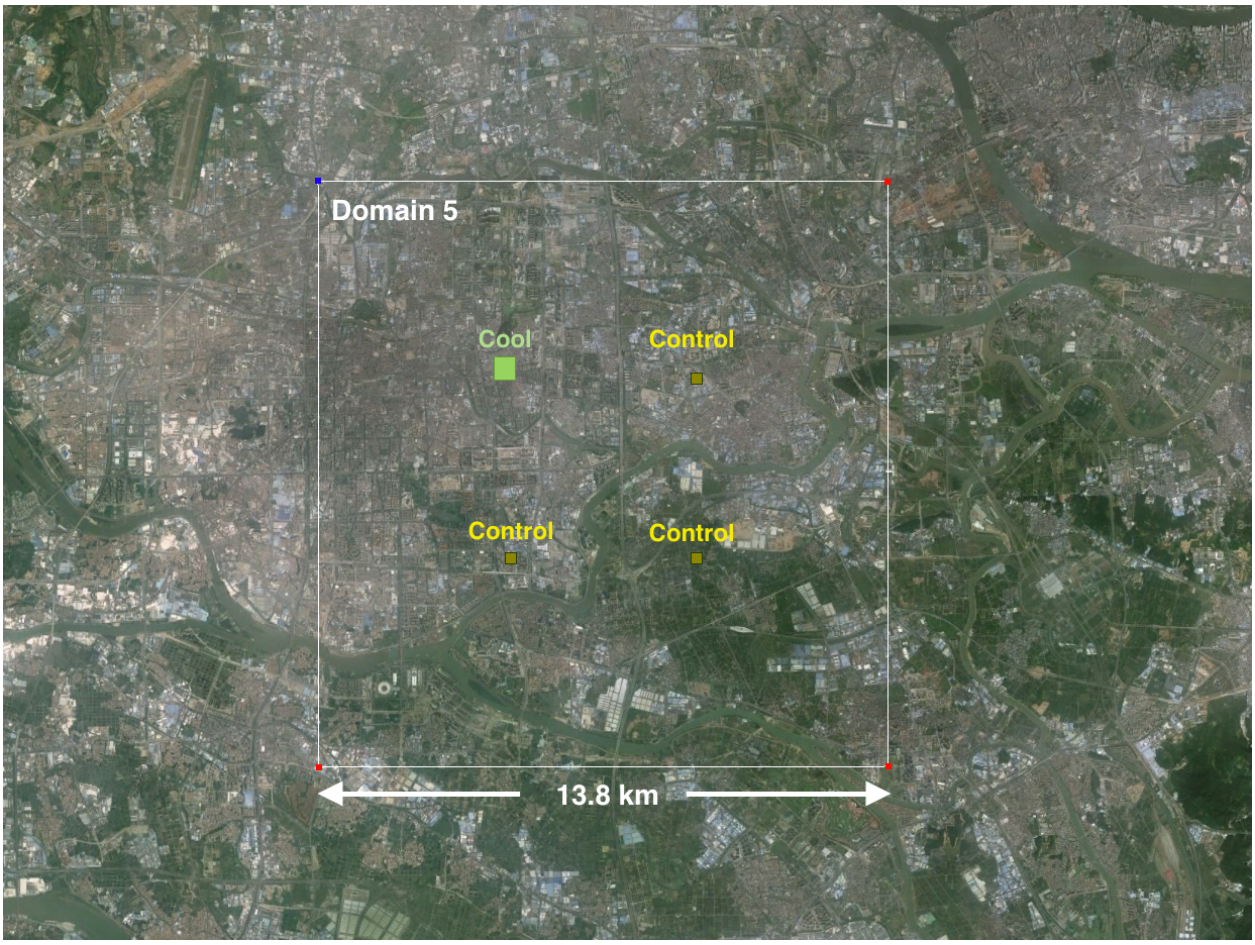

Figure 3. (a) The five nests of the model domain centered on Guangzhou, China. (b) Google Earth image of the fifth model domain, including the COOL and CONTROL areas for the upper left corner scenario.

A

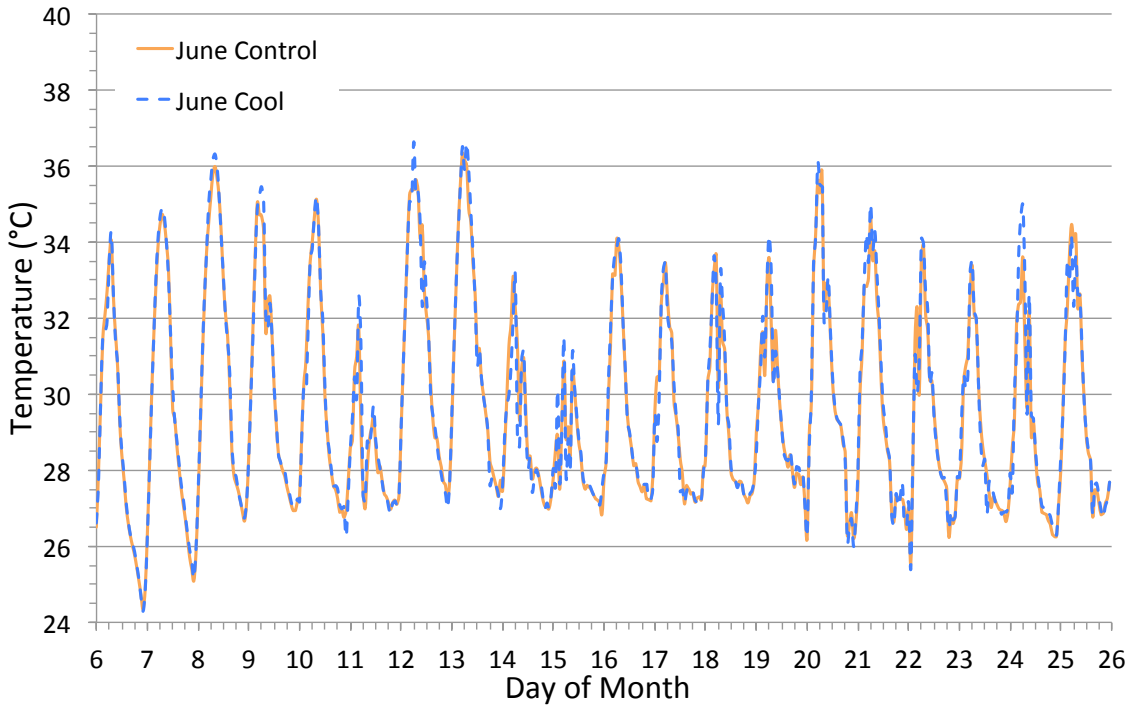

B

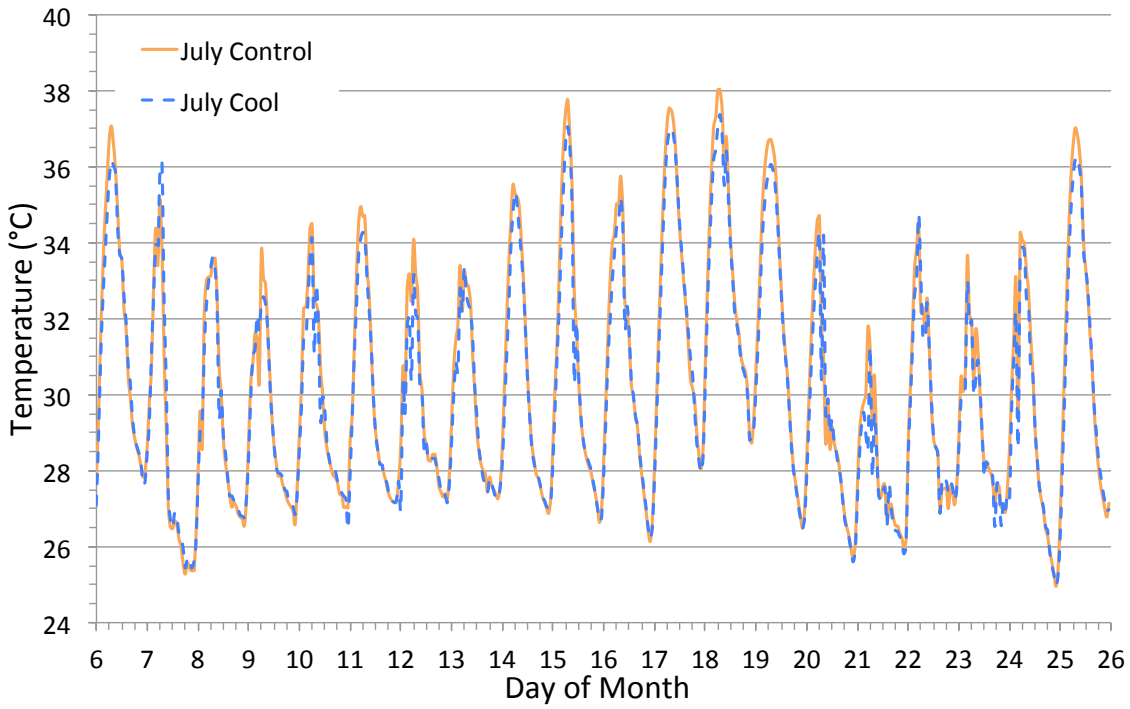

Figure 4. COOL and CONTROL hourly outdoor air temperatures at 2 m AGL in June and July.

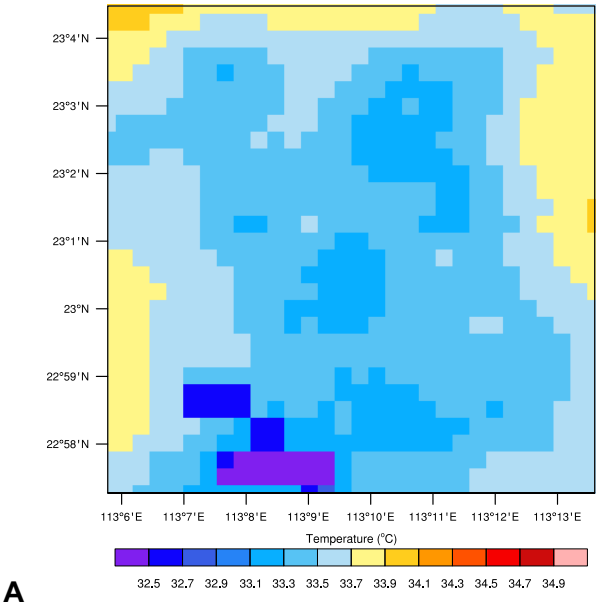
23°4'N
23°3'N
23°2'N
23°1'N
23°N
22°59'N
22°58'N
113°6'E
113°7'E
113°8'E
113°9'E
113°10'E
113°11'E
113°12'E
113°13'E
Temperature (°C)
32.5 32.7 32.9 33.1 33.3 33.5 33.7 33.9 34.1 34.3 34.5 34.7 34.9

A

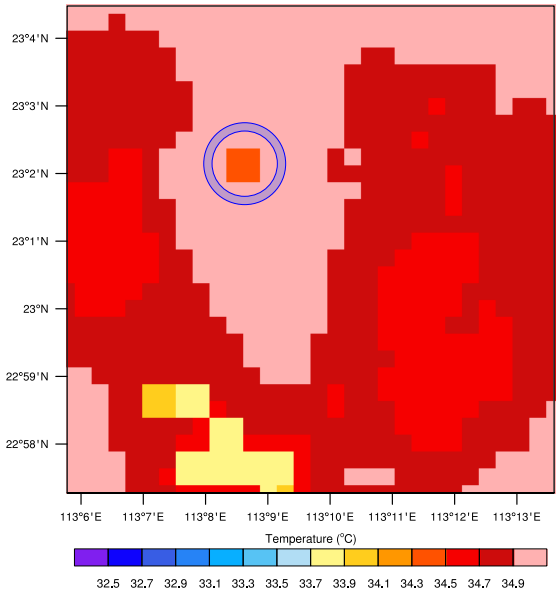
23°4'N
23°3'N
23°2'N
23°1'N
23°N
22°59'N
22°58'N
113°6'E
113°7'E
113°8'E
113°9'E
113°10'E
113°11'E
113°12'E
113°13'E
Temperature (°C)
32.5 32.7 32.9 33.1 33.3 33.5 33.7 33.9 34.1 34.3 34.5 34.7 34.9

B

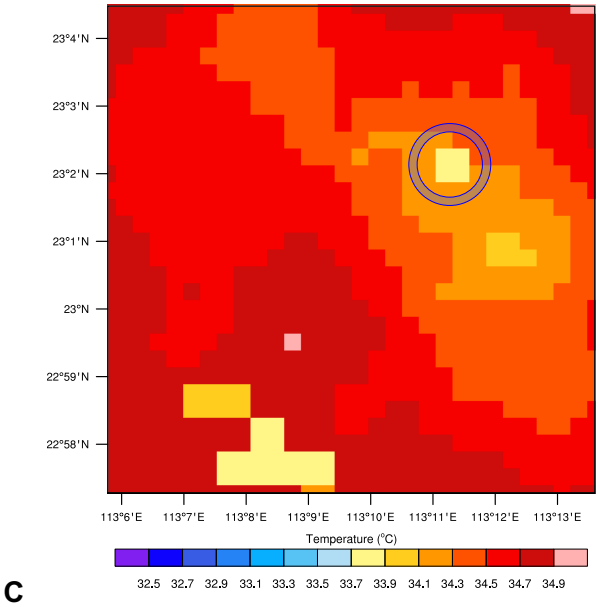
23°4'N
23°3'N
23°2'N
23°1'N
23°N
22°59'N
22°58'N
113°6'E
113°7'E
113°8'E
113°9'E
113°10'E
113°11'E
113°12'E
113°13'E
Temperature (°C)
32.5 32.7 32.9 33.1 33.3 33.5 33.7 33.9 34.1 34.3 34.5 34.7 34.9

C

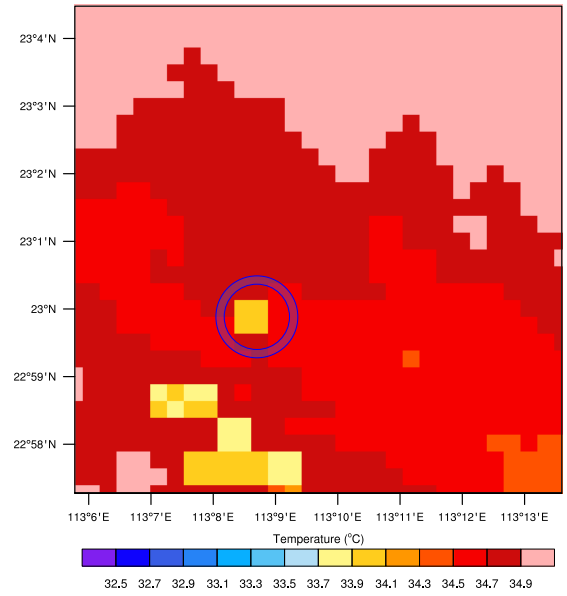
23°4'N
23°3'N
23°2'N
23°1'N
23°N
22°59'N
22°58'N
113°6'E
113°7'E
113°8'E
113°9'E
113°10'E
113°11'E
113°12'E
113°13'E
Temperature (°C)
32.5 32.7 32.9 33.1 33.3 33.5 33.7 33.9 34.1 34.3 34.5 34.7 34.9

D

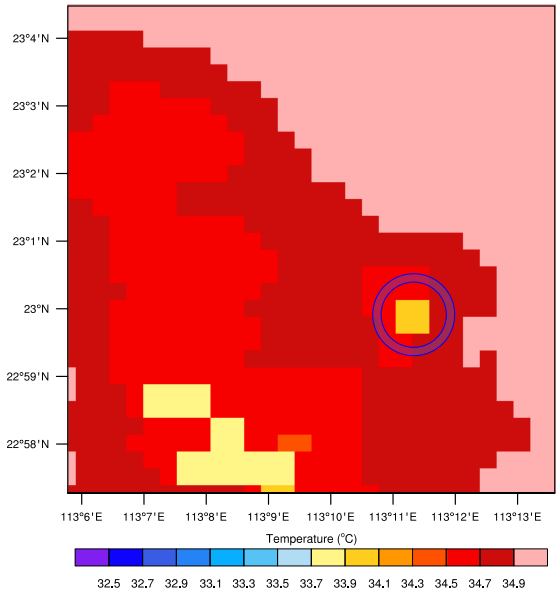

E

Figure 5. Average 2 m AGL outside air temperature at 2 pm LST for June (a) and separate July scenarios (b-e), with the COOL region clearly visible (and circled) in the July scenarios.

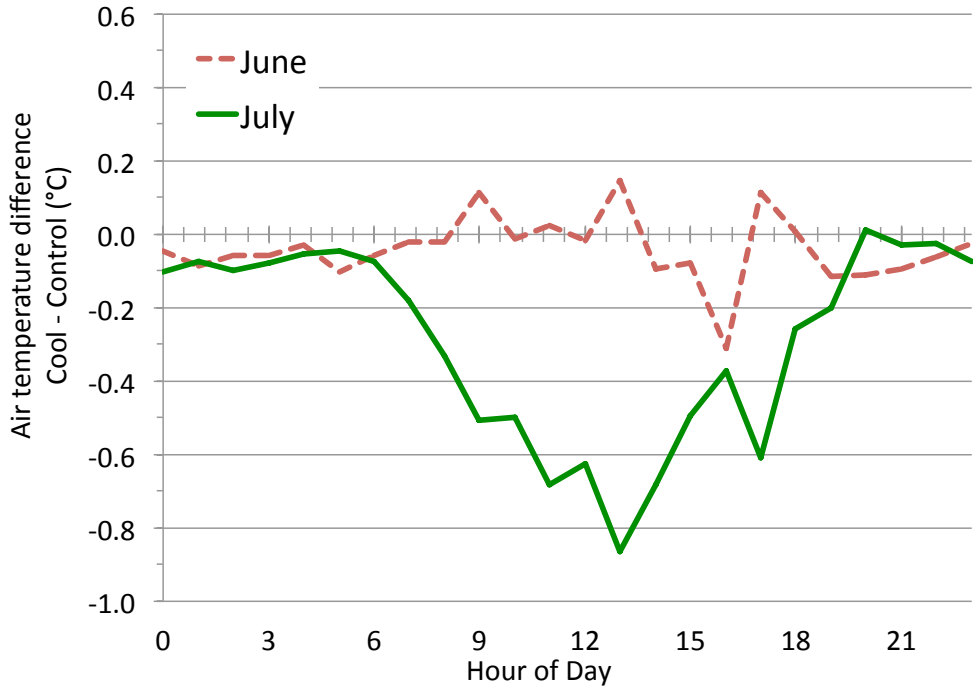

Figure 6. Average diurnal cycle of hourly temperature differences between COOL and CONTROL for June and July.

Appendix A: Hourly outdoor air temperatures in additional scenarios

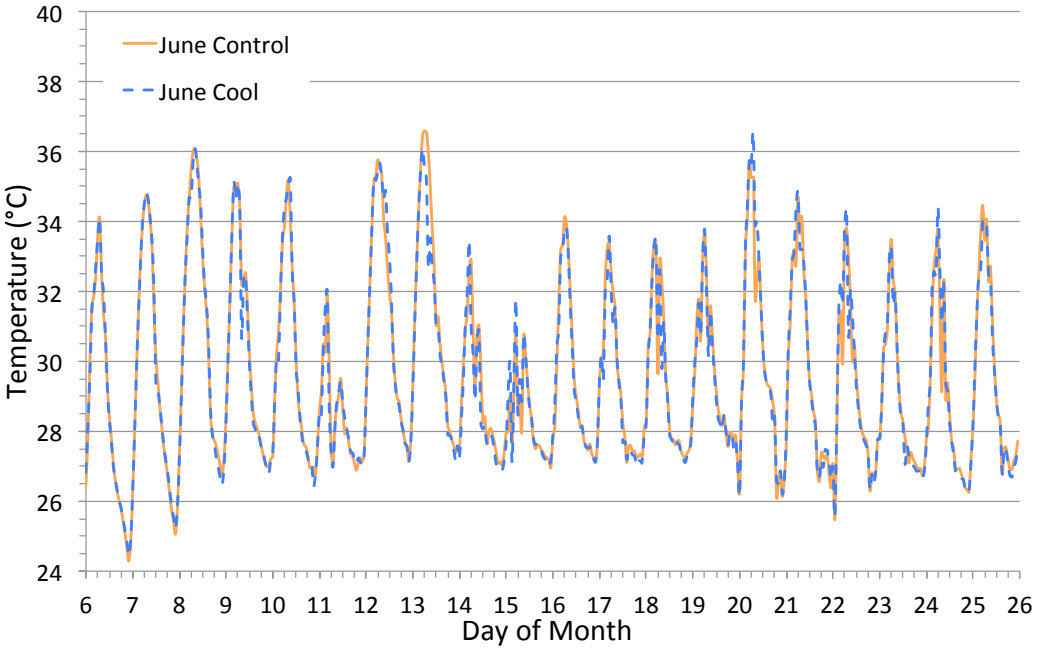

(a)

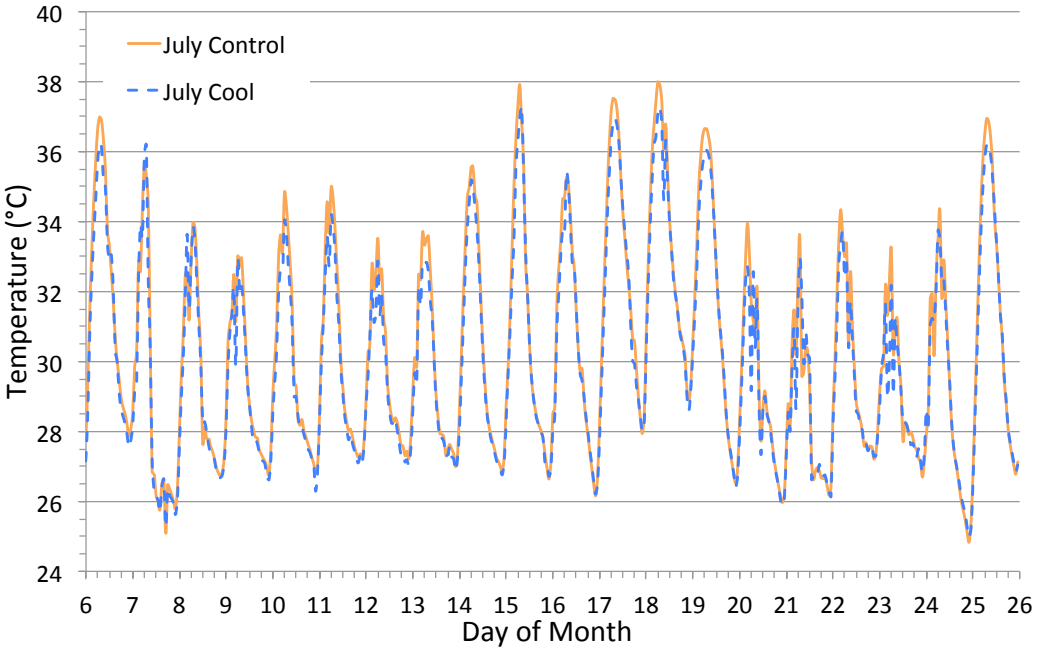

(b)

Figure A1. COOL and CONTROL 2 m AGL hourly outdoor air temperature for the lower-left corner scenario in June and July.

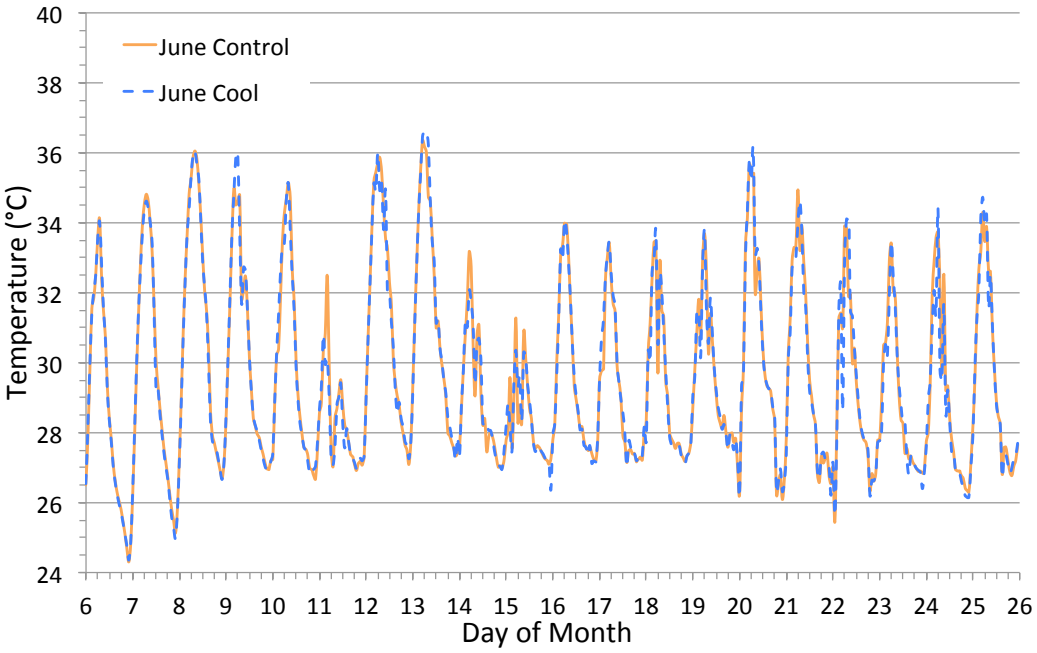

(a)

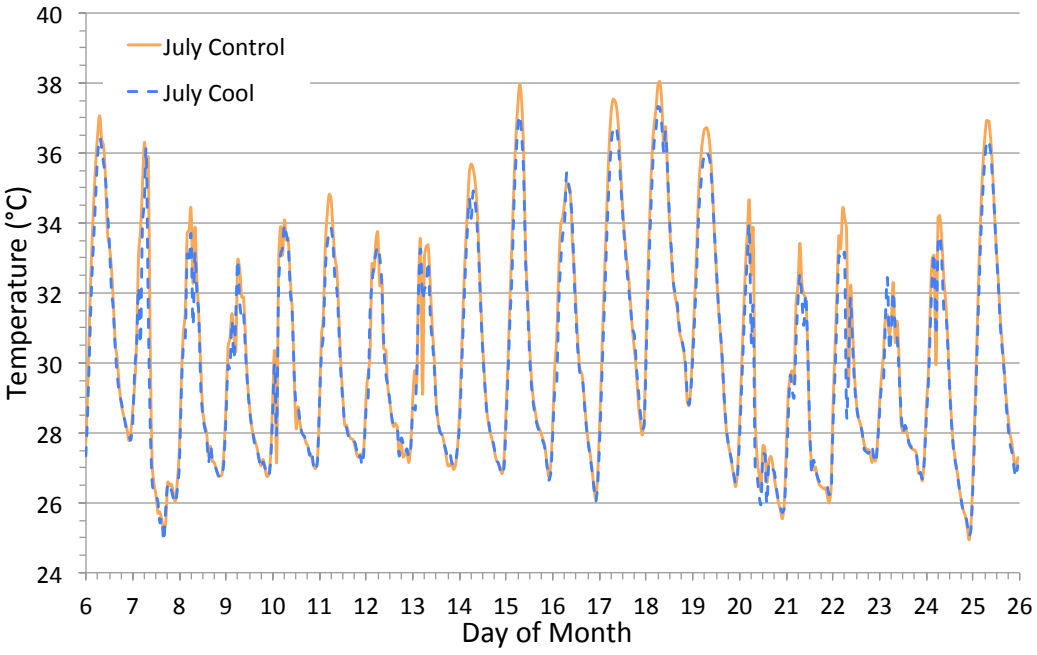

(b)

Figure A2. COOL and CONTROL 2 m AGL hourly outdoor air temperature for the lower-right corner scenario in June and July.

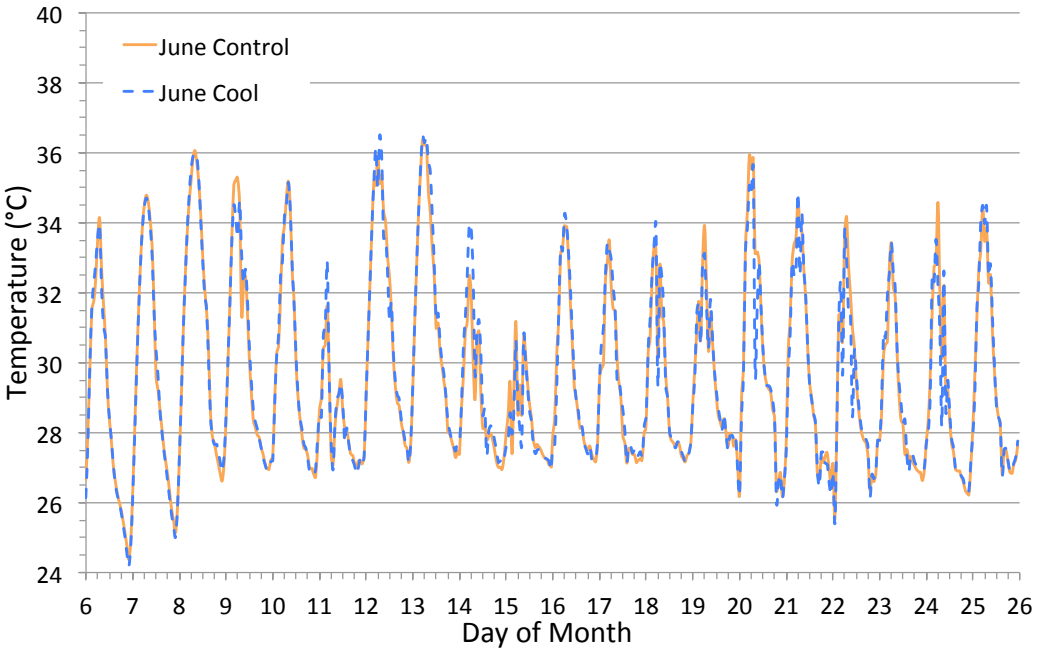

(a)

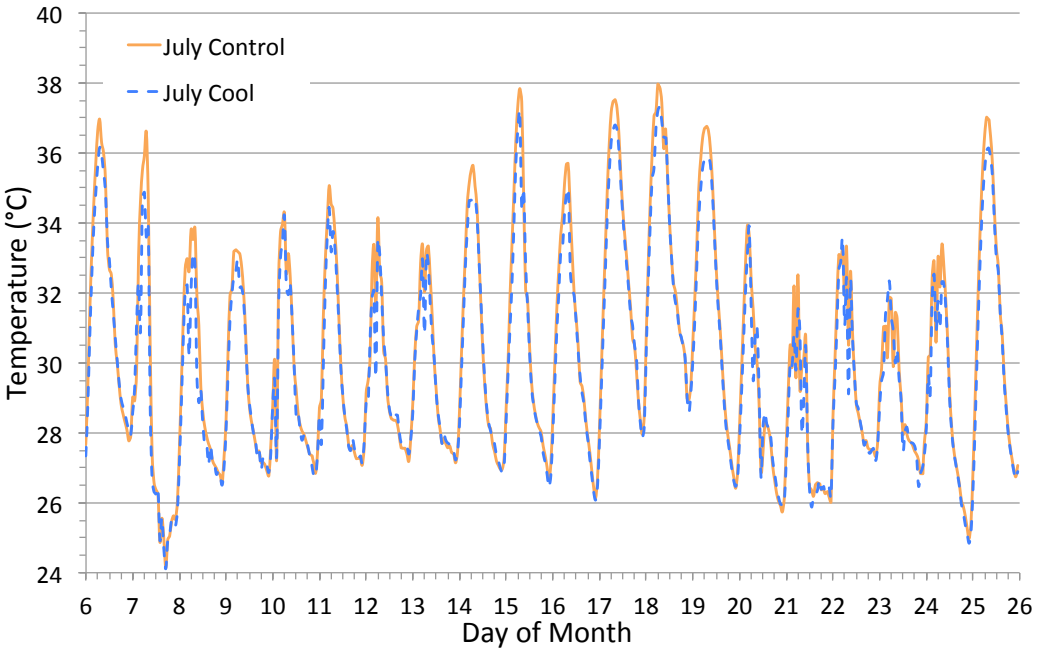

(b)

Figure A3. COOL and CONTROL 2 m AGL hourly outdoor air temperature for the upper-right corner scenario in June and July.

Appendix B: Average hourly temperature differences in additional scenarios

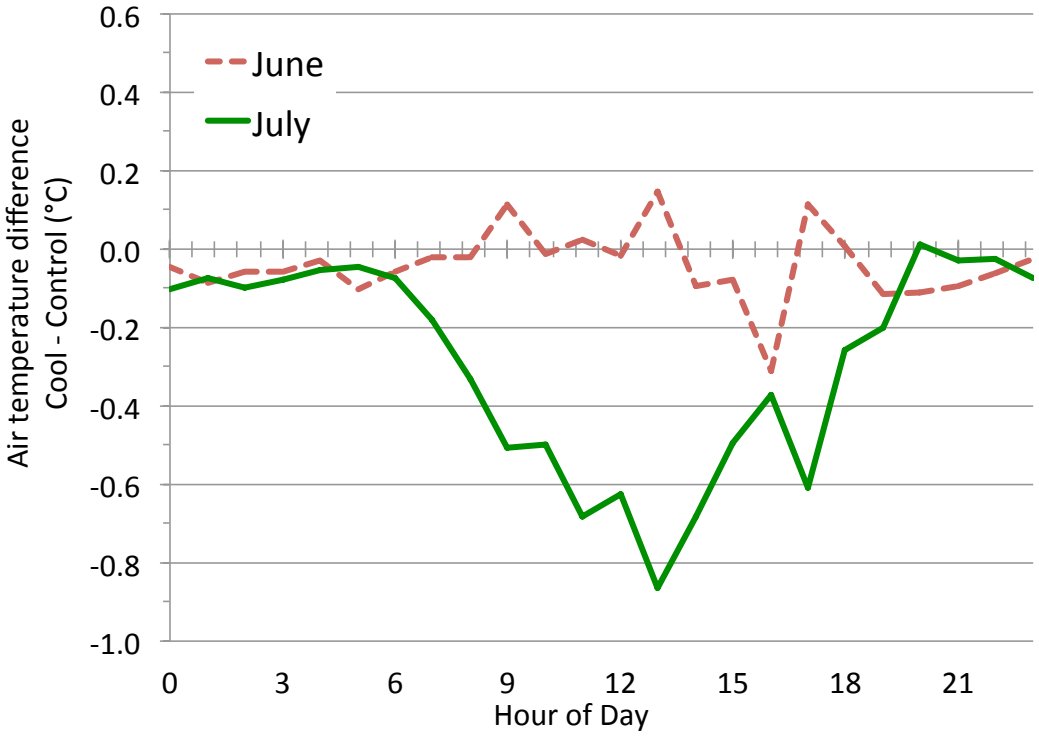

a)

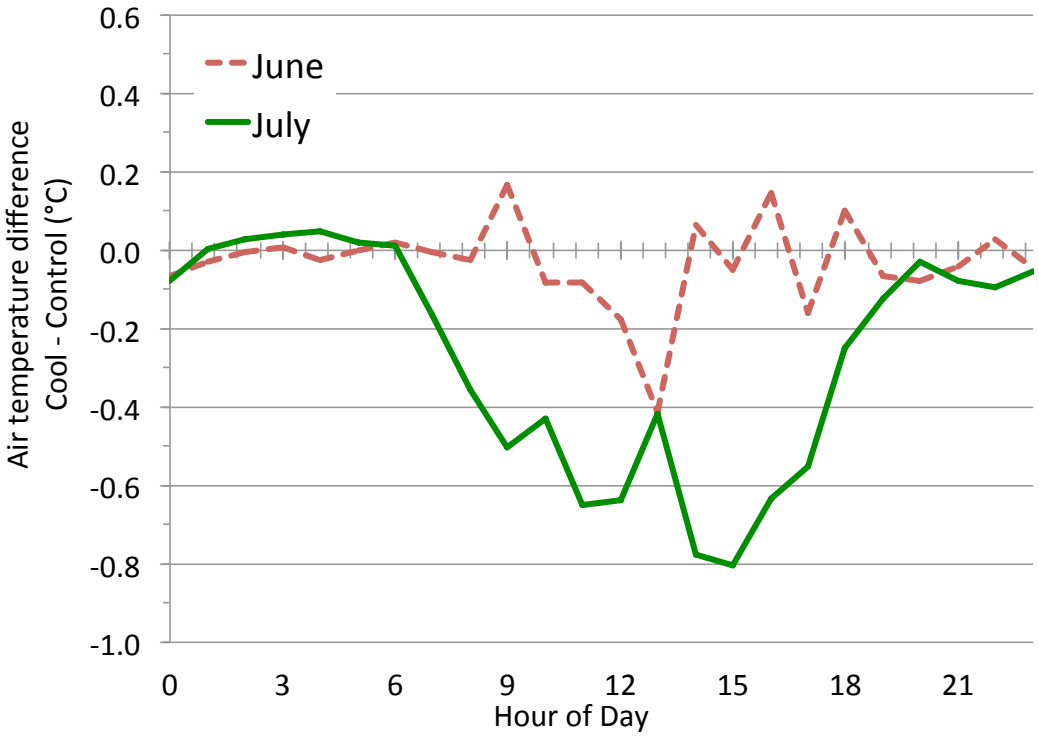

b)

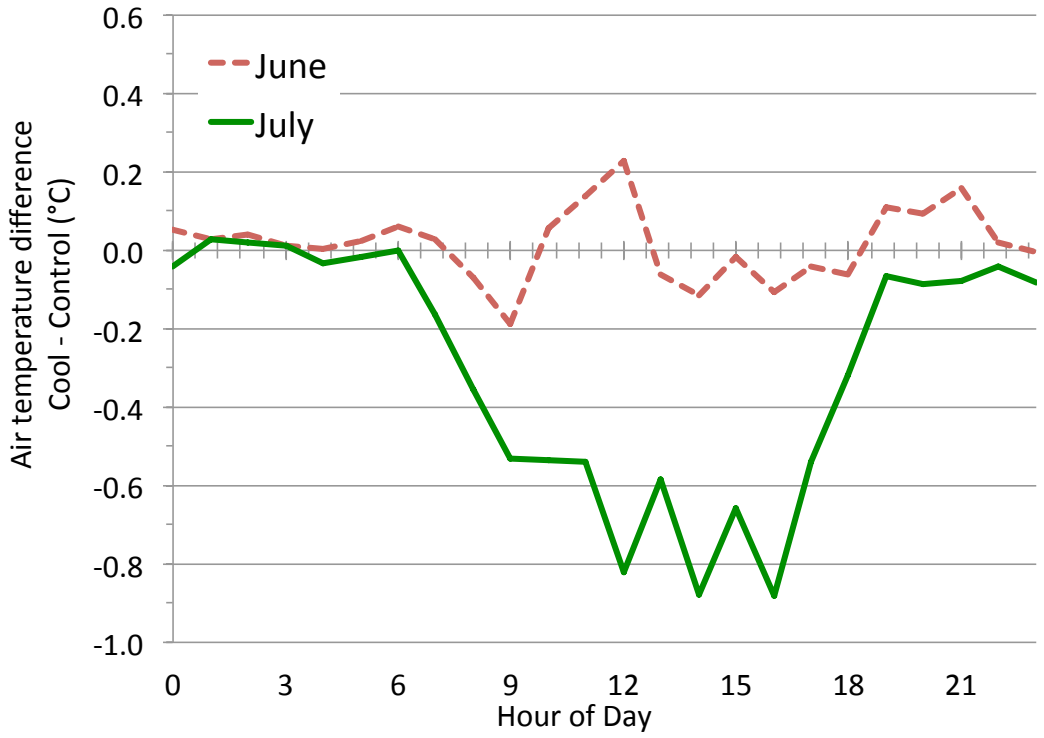

c)

Figure B1. Average diurnal cycle of hourly temperature differences between COOL and CONTROL for June and July for the (a) lower-left corner scenario, (b) lower-right corner scenario, and (c) upper-right corner scenario.